Available online at www.sciencedirect.com
ScienceDirect
Journal of Power Sources 161 (2006) 929–937
JOURNAL OF POWER SOURCES
www.elsevier.com/locate/jpowsour

AC impedance diagnosis of a 500 W PEM fuel cell stack Part II: Individual cell impedance

Xiaozi Yuan, Jian Colin Sun, Haijiang Wang *, Jiujun Zhang

Institute for Fuel Cell Innovation, National Research Council Canada, 4250 Wesbrook Mall, Vancouver, BC, Canada V6T 1W5

Received 6 June 2006; received in revised form 5 July 2006; accepted 6 July 2006
Available online 17 August 2006

Abstract

AC impedance or electrochemical impedance spectroscopy (EIS) has been demonstrated to be a powerful technique for characterizing and evaluating fuel cells. In this work, as an extension of our previous study on the stack impedance of a 500 W PEM fuel cell, we report the AC impedance studies on individual cells of the same fuel cell stack. The EIS of the stack with an active area of 280 cm^2 was measured at currents from 10 to 210 A in steps of 20 A using the combination of a FuelCon test station, a TDI loadbank and a Solartron 1260 Frequency Response Analyzer. Measurement of the individual cell EIS was carried out with the help of a rotary switch unit made in our lab. Two methods (floating mode and grounded mode) were utilized for measuring the impedance spectroscopy of the individual cells. The results show that both methods are applicable to individual cells. The results also indicate a good agreement between the total Ohmic loss in the stack and the combined Ohmic losses of the individual cells.

Keywords: AC impedance; Electrochemical impedance spectroscopy (EIS); Proton exchange membrane fuel cell (PEMFC); Stack; Individual cell

1. Introduction

Polarization curves and EIS are common techniques for evaluating the performance of a fuel cell and studying the factors that govern the electrochemical process within the fuel cells. Polarization curves provide a more direct measurement of fuel cell performance while EIS can provide richer information about the electrochemical processes within the fuel cell. EIS is a preferred technique in fuel cell diagnosis because:

- it can provide microscopic information about the electrochemical system;
- it allows modeling of the system with an equivalent circuit (EC);
- it has the capability to differentiate the individual contributions of each component, such as the membrane and gas diffusion electrode, to the fuel cell performance [1];
- it has the capability to differentiate the individual contributions of each process, such as interfacial charge transfer and mass transport in both the catalyst layer and backing diffusion layer, to fuel cell performance [2].

Due to the versatile capabilities of the EIS technique and the complexity of the membrane electrode assemblies (MEA) inside the fuel cell, EIS has been widely used to study fuel cell systems [3–8]. In various studies, EIS has been applied to:

- optimize the MEA structure including catalyst loading, polytetrafluoroethyline (PTFE) concentration [9], Nafion loading [10];
- optimize operation conditions [11–19];
- measure membrane resistance [20–25];
- study the effects of contaminates on fuel cells [26,27].

Its applications have ranged from single cells to fuel cell stack impedance [28,29] and localized impedance [30,31].

As summarized in our previous work [32], most of the previous studies have focused on single cells and only limited EIS work has been done on fuel cell stacks due to the cost and limitations of commercially available load banks. Furthermore, for a big industrial sized stack, measurement of only the stack EIS

* Corresponding author. Tel.: +1 604 221 3038; fax: +1 604 221 3001.
E-mail address: haijiang.wang@nrc.gc.ca (H. Wang).

0378-7753/$ – see front matter © 2006 Elsevier B.V. All rights reserved.
doi:10.1016/j.jpowsour.2006.07.020

would not generate the information required for understanding the detailed behaviour of individual cells. Even though the EIS of individual cells is a better tool for the evaluation of fuel cell stack performance, little work has been done to study individual cell behaviour within a large PEM fuel cell stack. It is known that Webb and Mϕller-Holst [33] measured the individual cell voltages in fuel cell stacks and Mennola et al. [34] studied the Ohmic voltage losses of the individual cells of a PEMFC stack with an active area of 25 cm^2 using a current interruption technique.

In the study of PEM fuel cells it is generally assumed that membrane resistance is independent of the current density [35–37]. But there have been reports that claim the value of membrane resistance increases with the current [21,25]. Apparently there are uncertainties regarding the effect of operating conditions on the resistance of the Nafion membrane [28], especially the membrane resistance at different current densities. The main objectives of this study are to present diagnostic information through AC impedance measurements of a 500 W PEM fuel cell stack, to measure the individual cell impedance spectra using multiple methods, to compare total Ohmic loss in the stack to the combined Ohmic loss of the individual cells, and to investigate current dependence of the membrane resistance using EIS.

2. Experimental

Impedance measurements were conducted on a 500 W PEM fuel cell stack. The stack tested in this study contained six cells, each with an active area of 280 cm^2. The test platform for AC impedance measurements of the fuel cell stack and individual cells consisted of an effective modification and combination of a FuelCon Evaluator-C 1 kW PEM fuel cell test station, a TDI WCL488 400-1000-12000 Water Cooled Electronic Load, and a Solartron 1260 Impedance Gain-Phase Analyzer. The experiments were performed in galvanostatic mode and the testing current was reached with the use of the water-cooled electronic load system (the load system used in this work has the capability of drawing 1000 A, which differs from the work of Ciureanu [28], where the measured maximum current was 100 A with a stack of 5 cells, whose geometric surface area was 250 cm^2). The inlet gases were H_2 in the anode and air in the cathode, and both gases had back-pressures of 1 bar (absolute pressure). The inlet hydrogen flow rate was maintained at 15 l min^{-1} and airflow was maintained at 80 l min^{-1} regardless of current density. Both the anode and cathode side were controlled at 100% relative humidity. All the measurements were carried out at 50 °C. Other experimental details can be found in our previous work [32].

The AC impedance spectra, including both phase shift and amplitude, were recorded as the frequency was scanned from 20 kHz to 0.1 Hz. Two connection methods, floating mode and grounded mode, were utilized for measurements of the EIS of the individual cells. Zplot was employed to measure the complex impedance data, and Zview was used for the electrochemical AC impedance data analysis.

The measurement of the individual cell EIS was made easier with the help of a homemade rotary switch unit. The electrical connection schematics for both of the EIS measurement methods employed in the study are depicted in Fig. 1. For the floating mode method, seen in Fig. 1(a), the Voltage 1 and Voltage 2 Low Input points of the impedance analyzer and the S-terminal of the TDI WCL488 Load-Bank were connected together as an individual voltage measuring point to connect to the negative end of a single cell in the stack. For the grounded mode method, seen in Fig. 1(b), the negative terminal of the stack was taken as the ground point and was always connected to the Voltage 2 Low Input point of the impedance analyzer and to #1 of the rotary switch unit. The cell switch unit had two 12-position rotary switches, switch #1 and #2. For the floating measurement mode, the two switches were moved together to connect to the individual cell. For the ground referenced measurement mode, the switch #1 was fixed to P1 (the stack negative terminal) and the switch #2 was moved to different positions to connect different cells, i.e., 1 cell, 2 cells, and up to 6 cells (counted from the anode side).

Due to the drift of the system being measured, the fuel cell stack was operated at 100 A (individual cell potential was about 0.6 V) for at least 1 h in order to achieve a steady-state environment before starting the impedance measurement. The system drift resulted from various mechanisms, such as adsorption of solution impurities, growth of an oxide layer, build-up of reaction products in solution, coating degradation, and temperature changes. The total Ohmic resistance in the stack was measured or calculated before and after the individual measurements to verify the reliability of the measurements.

3. Results and discussion

3.1. Selection of the signal amplitude

AC impedance is measured in either the potentiostatic mode (voltage control mode) or galvanostatic mode (current control mode). The galvanostatic mode is preferred because PEM fuel cell performance tests, i.e., polarization curves, are usually carried out in galvanostatic mode and current control is easier with commercial loadbanks than voltage control. In addition, the galvanostatic mode forces a constant conversion rate with respect to the charged species [38].

The amplitude used for the AC signal, which determines the signal/noise (S/N) ratio, plays an important role in obtaining good impedance spectra. Wagner et al. [38] conducted their AC impedance measurements in galvanostatic mode. They used a 200 mA amplitude AC signal superimposed onto a DC current of 5 A (current density: 217 mA cm^{-2}) to study the change of electrochemical impedance spectra with time during CO-poisoning of the Pt-anode in a membrane fuel cell. In Jaouen and coworkers work [39,40], the authors maintained the amplitude of the AC current at 5% of the DC current.

In this work, AC signals of different amplitudes were tested to find the optimal choice. Fig. 2 shows the effect that different amplitudes of the AC signal have on the spectra at a 50 A DC current. The amplitudes studied here are from 1% to 15% of the DC current. Two semicircle loops were observed in the spectra. The high frequency loop starts at a frequency of 20 kHz, and ends at around 1 kHz, which is associated with the internal Ohmic

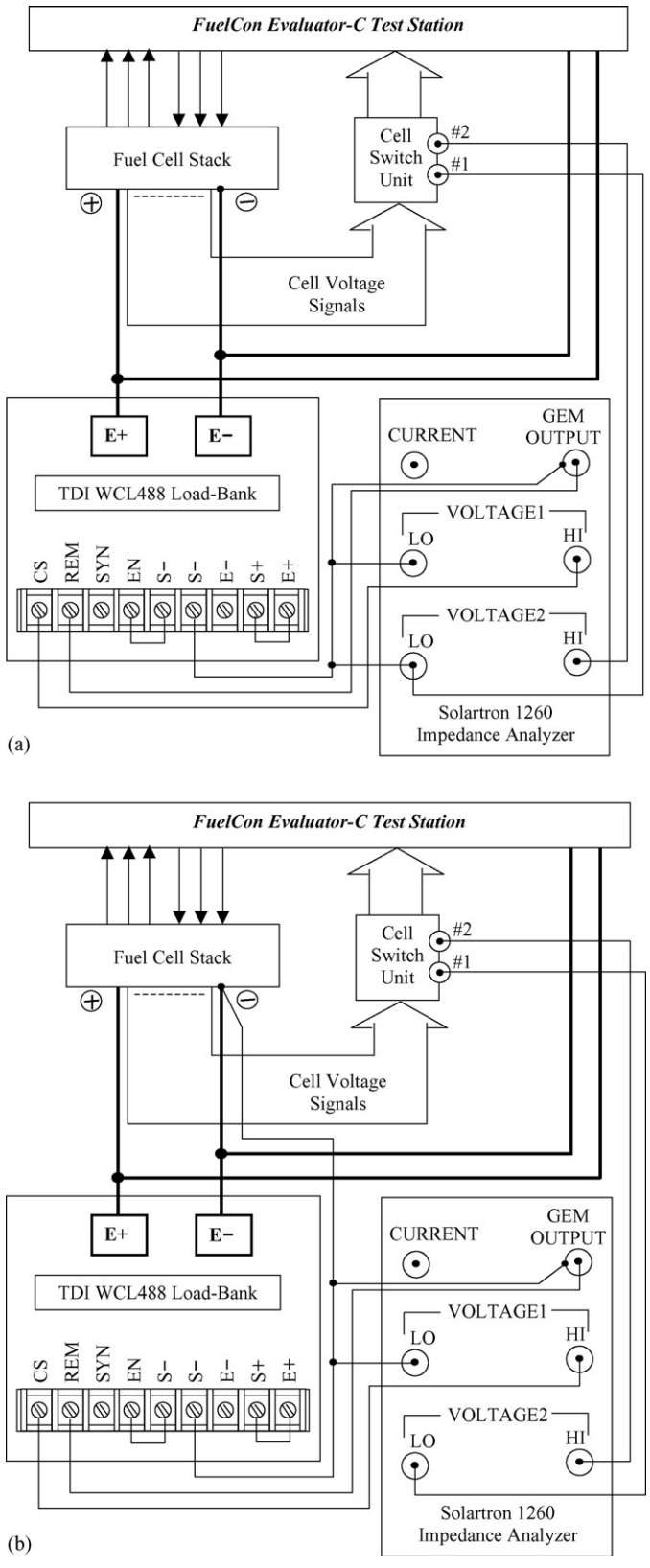

Fig. 1. Electrical connection schematics of the EIS measurement. (a) The floating mode and (b) the grounded mode.

resistance and the contact capacitance in the granular electrode structure of the MEAs or issues related to the measurement circuits [32]. The low frequency loop, called the "kinetic loop", starts at a frequency of approximately 1 kHz and ends at around 0.3 Hz with a peak frequency of 7.54 Hz, which corresponds to the charge transfer kinetics of the Oxygen Reduction Reaction (ORR) at the electrode interface.

As seen in Fig. 2(a and b), there is almost no difference between the spectra of the high frequency portion when AC signals of different amplitudes in the range from 1% to 15% are applied. On closer examination of the low frequency region, depicted on the right sides of Fig. 2(a and b), one can see that at low frequencies, the data points are scattered for amplitudes of 1%, 2% and 3%. Smooth curves are observed when the amplitudes of the AC signal are larger than 5%. Further increase of the AC signal amplitude from 5% to 10% and 15% results in a tiny expansion of the kinetic loop, seen in Fig. 2(b). Similar trends are also observed in the AC impedance spectra measured at DC currents of 100 and 150 A, as illustrated in Figs. 3 and 4 with the characteristic frequencies marked. The only difference is that at the low frequency portion, the impedance curves shrink when the AC signal amplitude increases from 5% to 10% and 15%. At this moment, there is no clear understanding of the cause for the difference observed. As pure speculation, it might be related to the contribution of mass transport to the total impedance. Nevertheless, the objective is to select the AC signal amplitude that least affects the measurement results and has low noise. From this work, it appears that the AC signal with amplitude of 5% of the DC current is a reasonable choice. This choice is in agreement with the work of Jaouen and co-workers. They used the AC current amplitude of 5% of the DC current [39,40]. Hence, the following experiments are all measured with AC current amplitude of 5% of the DC current.

3.2. Measurement results in grounded mode

In the grounded mode measurements, AC impedance spectra were measured in the order of first cell, first two cells, first three cells, and continued in this way until the impedance of the whole stack was measured. The advantage of this method was that the instrument could be grounded and the stack impedance was measured when the impedance of all the cells was measured. The disadvantage was that individual cell impedance, except for the first cell, was not measured directly. Rather, individual cell impedances were obtained by subtracting the measured impedance from the impedance of the cells in front of the cell investigated.

The AC impedance that was measured in the grounded mode at a DC current of 50 A is presented in Fig. 5. The cells were counted starting from the anode side of the stack. Seen in Fig. 5, as the number of cells measured increased, the kinetic loop and the high frequency intercept of this kinetic loop also increased. The impedance of individual cells was obtained from these measurements by subtracting the measured impedance from the impedance of the cells in front of the cell studied. Further processing of the impedance data was carried out using the Solartron software, Zview.

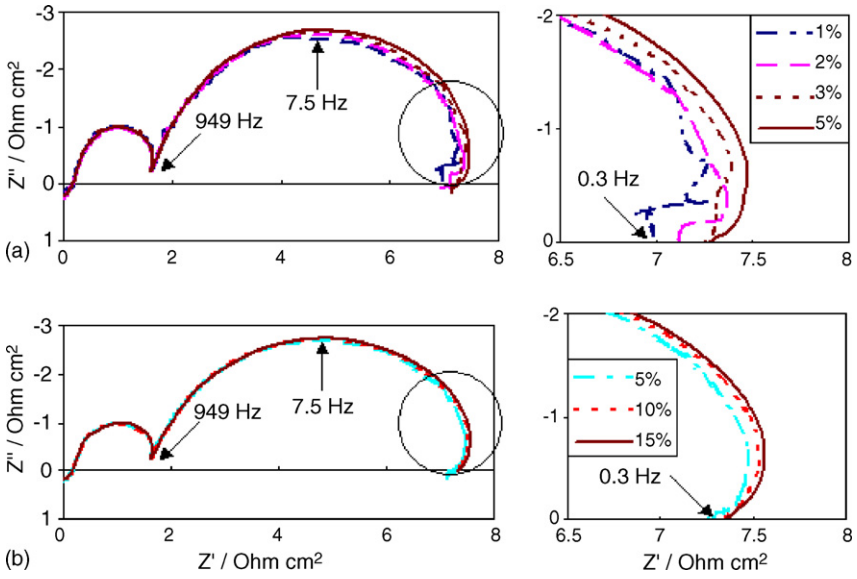

Fig. 2. The effect of AC amplitude on the Nyquist plots at DC current of 50 A at 50 °C with the low frequency region enlarged on the right side. The value of AC amplitude is (a) 1–5% and (b) 5–15% of DC current.

It is known that in the Nyquist plot, the high frequency intercept of the kinetic loop and the real impedance axis is a measure of the total Ohmic resistance of the cell. The total resistance can be expressed as a sum of the contributions from contact resistances and Ohmic resistances of the cell components including membrane, catalyst layer, gas diffusion layer and bipolar plate [41], among which, the biggest contributor is the membrane resistance. Accurate values for the high frequency intercept of the kinetic loop and the real impedance axis can be obtained by fitting the impedance data to an appropriate equivalent circuit.

During the data fitting process only the kinetic loop was used with an equivalent circuit. The semicircle at the high frequency region, as seen from Figs. 2–5, was not included because this semicircle at the high frequency region is not associated with the electrode process [32]. Since there was almost no overlap of the two loops, the high frequency semicircle had a minimal effect in the data fitting process. The results obtained after this data processing are illustrated in Figs. 6 and 7.

Fig. 6(a) shows the Ohmic resistance of the individual cells at different currents and 50 °C, while Fig. 6(b) shows the comparison of the stack Ohmic resistance to the sum of the individual cell Ohmic resistance. It is seen clearly that at low currents, with increasing current, the Ohmic resistance decreases. At high currents, however, the Ohmic resistance does not vary much. There is only a minor fluctuation that is most likely due to experimental error. Among the different cells, there is no clear trend shown in the Ohmic resistance data. In most cases, however, it appears that the cells in the center have lower Ohmic resistance. The cen-

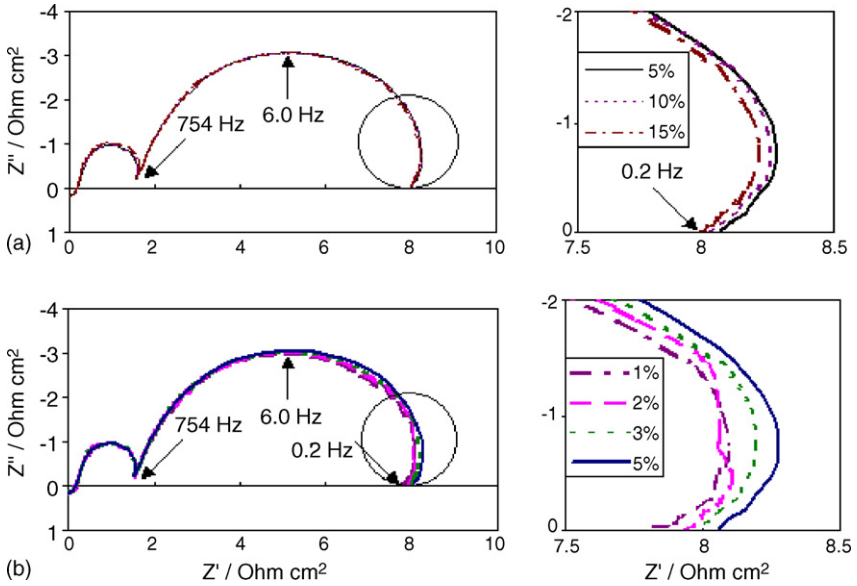

Fig. 3. The effect of AC amplitude on the Nyquist plots at DC current of 100 A at 50 °C with the low frequency region enlarged on the right side. The value of AC amplitude is (a) 5–15% and (b) 1–5% of DC current.

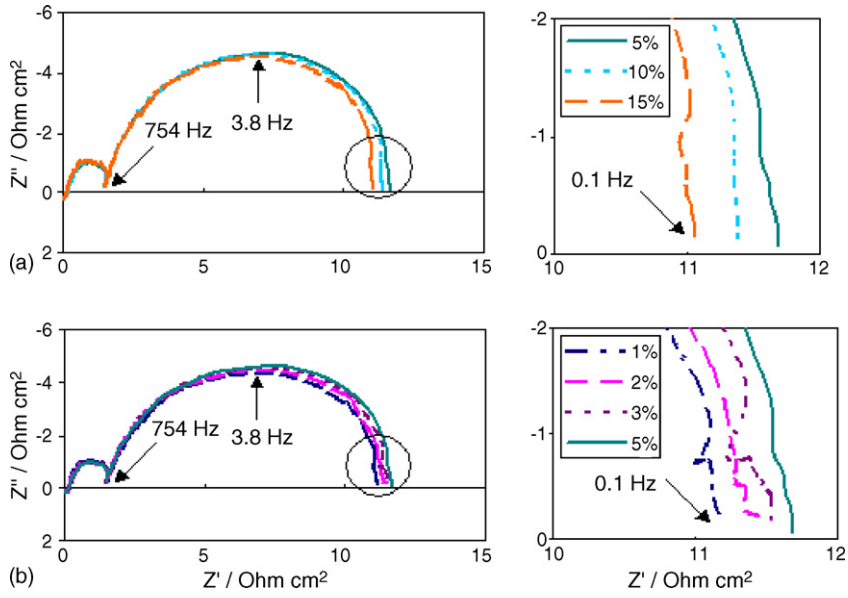

Fig. 4. The effect of AC amplitude on the Nyquist plots at DC current of 150 A at 50 °C with the low frequency region enlarged on the right side. The value of AC amplitude is (a) 5–15% and (b) 1–5% of DC current.

ter cells can probably reach a slightly higher temperature than the end cells due to the effect of thermal radiation, resulting in a higher conductivity hence lower Ohmic resistance of the membrane (which is known the major contributor to the total Ohmic resistance). This result agrees with Mennola et al. [34]. It also appears that the variance of the Ohmic resistance among the individual cells is small at high currents but relatively large at low currents. It suggests that at low currents the temperature and hydration of the membranes can vary widely from cell to cell. This could result in faster membrane degradation of some cells than others. Membrane degradation is known as one of the predominant failure modes for PEM fuel cells. Large variance of Ohmic resistance at low currents will eventually affect the durability of the fuel cell stack.

Freire and Gonzalez [42] measured the Ohmic resistances at different currents by AC impedance through the high frequency intercept values of the kinetic loops. Their results indicated that the Ohmic resistances, mainly membrane resistances as aforementioned, change with current. Slade et al. [21], who used the

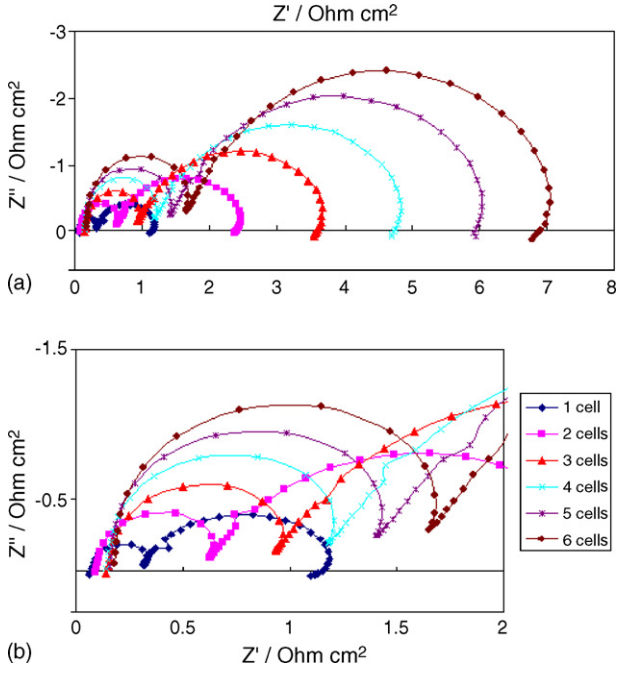

Fig. 5. The typical impedance spectra in the way of common-point connection (grounded mode) at DC current of 50 A at 50 °C. The cells are counted starting from the anode side of the stack. (a) Full screen of Nyquist plot and (b) enlargement of the high frequency region.

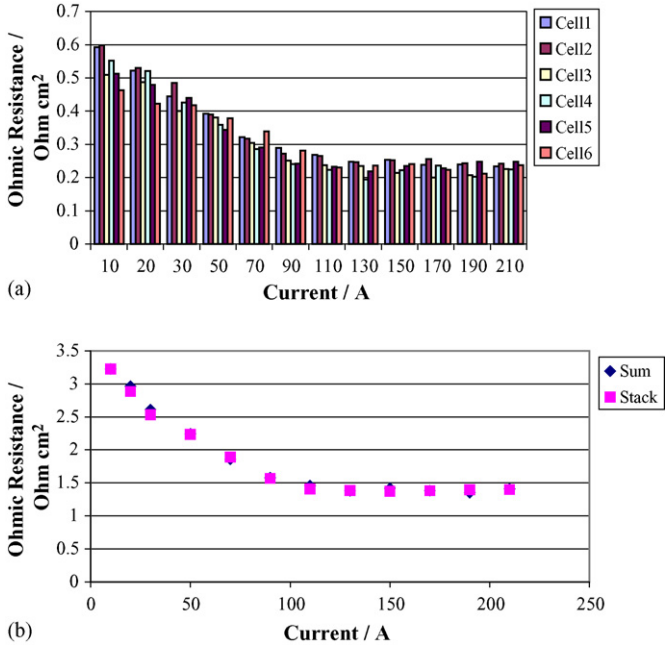

Fig. 6. (a) Ohmic resistance of the individual cells at different currents at 50 °C. Measurement mode: grounded. (b) Comparison of stack Ohmic resistance and the sum of the unit cell Ohmic resistance. Measurement mode: grounded.

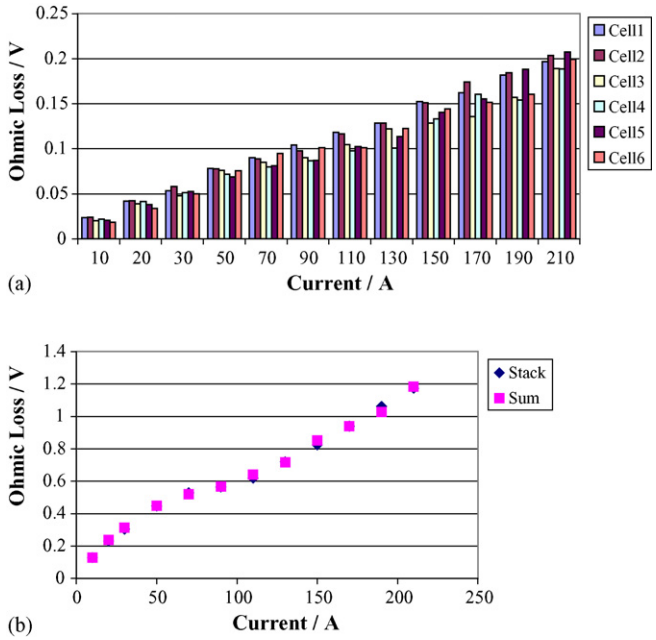

Fig. 7. (a) The change in Ohmic loss of individual cells with current at 50 °C. Measurement mode: grounded. (b) The comparison of the stack Ohmic loss with the sum of the unit cell Ohmic loss. Measurement mode: grounded.

current interruption method to measure membrane resistance as a function of current density, made similar observations. Their experiments were carried out with a Ballard Mark 5E single cell. The cell was operated with internally fully humidified H_2/O_2 at 3 bar and 1.5/10.0 stoichiometry. The results showed that the area resistance as a function of current is flat for thinner membranes. But when the membrane thickness increased, the area resistance increased substantially at high current densities. They suspected that this increase of membrane resistance at high current densities for thicker membranes was due to drying of the membrane at the anode. Andreaus and Scherer [25] used both the current pulse technique and AC impedance to study the current dependence of membrane resistance. In their experiments, both gases were fed in 50% excess. The electrode active area was 28 cm^2. The results showed that membrane resistance increased significantly at high current densities, thus causing a performance loss as predicted by various models [43–45]. According to the models, membrane resistance increased with current. They explained that at medium and high current densities, the decrease in water content started to become significant due to electro-osmotic drag. This resulted in the increase of the specific membrane resistivity of the anode portion [46]. Thus, it gave rise to an increase of the total membrane resistance. This effect was more pronounced for electrolyte membranes with unfavorable water back-transport characteristics, such as thick membranes or membranes with high EW.

Our results seem to be in discrepancy with the literature. The membrane resistance we obtained decreased with current rather than increasing. The reason was that in our experiments we kept the flow of inlet gases unchanged for the duration of the measurements. Therefore, membrane humidification at low currents was possibly insufficient due to the large flow of gases and small amount of water produced at the cathode. At high currents, humidification increased due to larger amounts of product water. This demonstrated that the AC impedance method is a very sensitive technique for detection of membrane hydration.

The results in Fig. 6(b) indicate a good agreement between the total Ohmic loss in the stack and the combined Ohmic loss of the individual cells. A similar trend is observed with the stack Ohmic resistance at different currents, as seen already for the individual cells.

The calculated voltage loss due to Ohmic resistance for each cell at different currents is presented in Fig. 7(a). It is seen that the Ohmic voltage loss increases approximately linearly with current, although the Ohmic resistance is not constant at the different currents. A similar trend is visible in Fig. 7(b), which compares the stack Ohmic voltage loss and the sum of the Ohmic voltage loss of individual cells. This result explains why many researchers have the perception that membrane resistance is constant regardless of current. Many researchers try to obtain the in situ membrane resistance through the analysis of polarization curves. Due to the fact that Ohmic voltage loss changes linearly with current, there is a natural assumption that membrane resistance does not change with current. This assumption can only be shown wrong through AC impedance measurements.

At high currents, a small variation in Ohmic resistance can cause a large variation in voltage loss due to the Ohmic resistance. This phenomenon is seen in Fig. 7(a) where the variation in Ohmic voltage loss at high currents is much bigger than that at low currents. Therefore at high currents, it is more likely to have "low cells", which have a tremendous impact on the reliability of a fuel cell stack.

It is known that the diameter of the kinetic loop in the Nyquist plot is associated with charge transfer resistance. Therefore, in addition to the Ohmic resistance, charge transfer resistances can also be obtained from the same spectra of the impedance measured [32]. Fig. 8(a) shows the dependence of the charge transfer resistance of individual cells on current. At low currents the charge transfer resistance is observed to decrease with increasing current, due to the increased driving force for the electrode process. Then, at about 100 A, it begins to rise due to the increasing contribution of mass transport [32]. This trend is more obvious in Fig. 8(b), which shows the dependence of the stack charge transfer resistance on current.

3.3. Results by floating mode measurement

The floating mode method is able to measure the AC impedance spectra of each individual cell directly. The advantage of this method is that the data analysis is not as time-consuming as that of the grounded mode method.

In our measurements, at each current, the measurements began with the whole stack, then the individual cells, and then the whole stack again. In this way we were able to check the reliability of the measurement system and we could compare the sum of the Ohmic losses of the individual cells to the Ohmic loss measured across the whole stack. The noise level of the spectra measured, fortunately, was quite acceptable. Similar data processing protocols were used and the results are depicted in

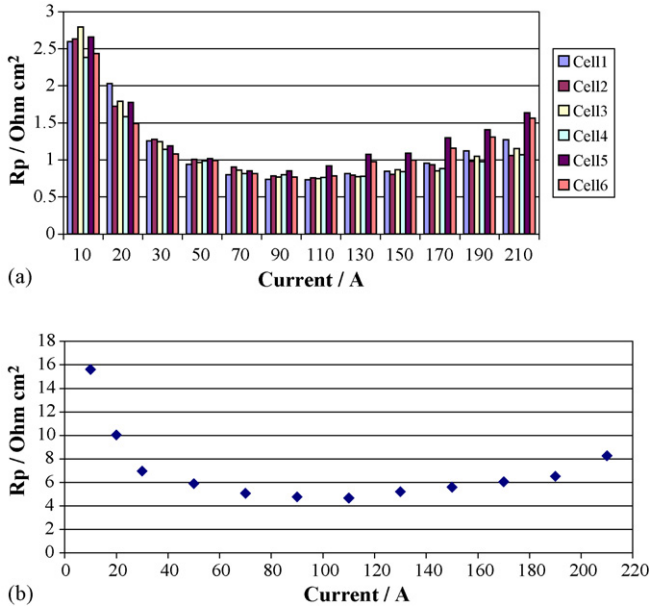

Fig. 8. (a) The charge transfer dependence of individual cells on currents. Measurement mode: grounded. (b) The charge transfer change dependence of the stack on current. Measurement mode: grounded.

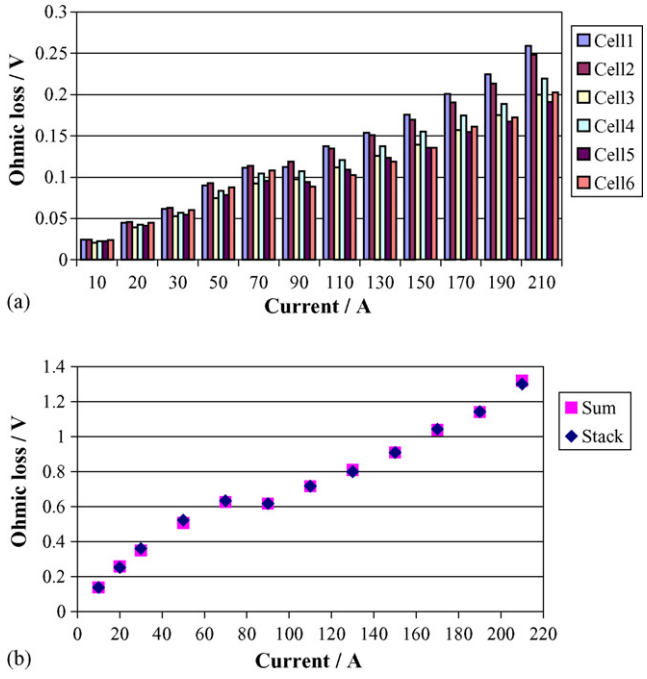

Fig. 10. (a) Comparison of stack Ohmic resistance and the sum of the individual cell Ohmic resistance. Measurement mode: floating. (The Ohmic resistance of the stack is the average value of measurements taken before and after the individual cell measurements.) (b) Comparison between the stack Ohmic loss and the sum of the unit cell Ohmic loss. Measurement mode: floating. (The Ohmic loss of the stack is the average value of measurements taken before and after the individual cell measurements.)

Figs. 9–11. Fig. 9(a) shows the Ohmic resistance of the individual cells measured at different currents at 50 °C, and Fig. 9(b) shows a comparison of stack Ohmic resistance and the sum of the individual cell Ohmic resistances. The calculated Ohmic voltage loss of the individual cells at various currents is depicted in Fig. 10(a). The comparison of stack Ohmic voltage loss and the sum of the individual cell Ohmic voltage losses is illustrated in Fig. 10(b). The charge transfer resistance of individual cells at

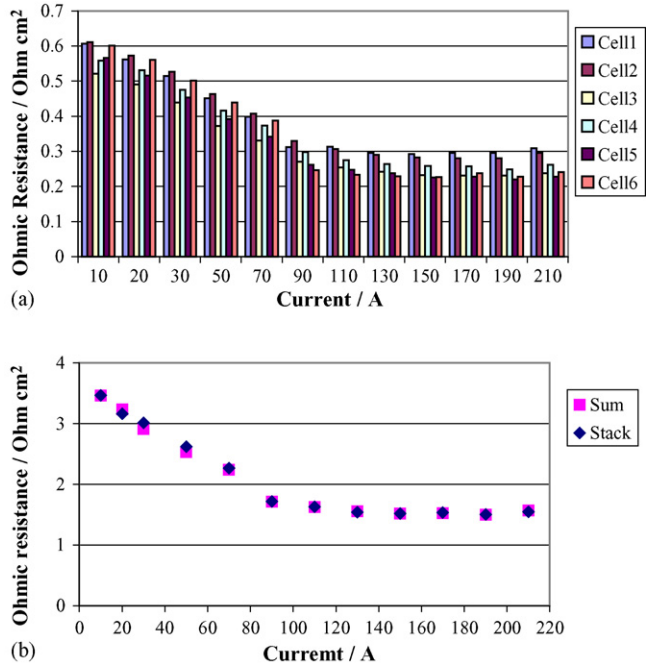

Fig. 9. (a) Ohmic resistance of the individual cells at different currents at 50 °C. Measurement mode: floating. (b) The change in Ohmic loss of individual cells with current at 50 °C. The measurement mode: floating.

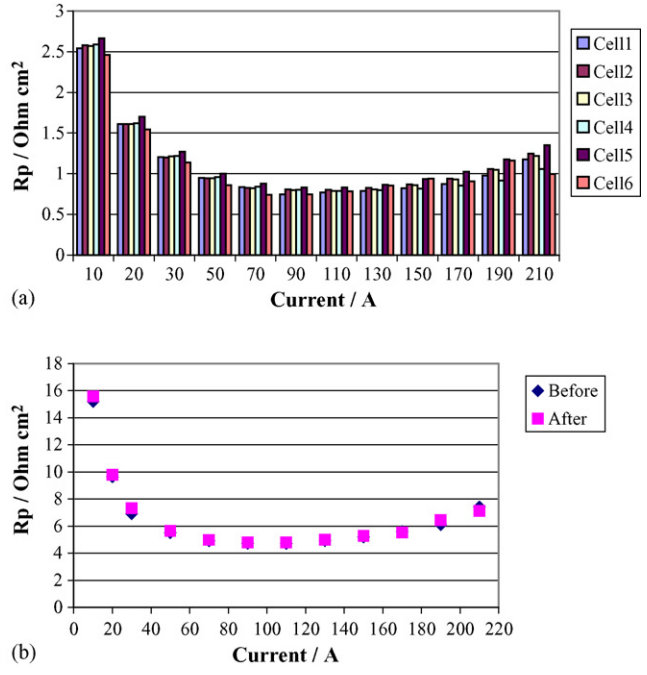

Fig. 11. (a) The charge transfer dependence of individual cells on currents. Measurement mode: floating. (b) The charge transfer change dependence of the stack on current. Measurement mode: floating.

various currents is presented in Fig. 11(a and b) shows the dependence of the stack charge transfer on current before and after the individual cell measurement, which indicates the reliability and stability of the measurement system.

Comparing Figs. 9–11 with Figs. 6–8, respectively, one can easily find that the two methods generate almost identical results. Only a small difference in the individual cell resistances by the two different measurement methods is noticed, which may be attributed to the variations of the individual cells during the measurement or might be purely experimental error. Nevertheless, this small difference will not alter the conclusions from these measurements. In summary, either of the two measurement methods can be used in obtaining individual cell impedance spectra.

4. Conclusion

The EIS of the individual cells of a 500 W PEM fuel cell stack can be measured in galvanostatic mode with the combination of a FuelCon test station, a TDI loadbank, and a Solartron 1260 Frequency Analyzer using either a grounded connection or a floating connection. The noise level for the floating connection measurements is not a concern. The optimum choice for the amplitude of the AC signal is about 5% of the DC current.

In general, there are two semicircular loops shown in the Nyquist plot for the individual cell impedance spectra measured. The loop at the lower frequency region corresponds to the electrode process. The loop at the higher frequency region is not associated with the electrode process and can be excluded during the equivalent circuit fitting process. The Ohmic resistance extracted from the AC impedance spectra shows a trend to decrease with current, which is contradictory to some of the previous studies. This is attributed to the particular experimental condition used. Presently, further investigation is being carried out using current interruption and EIS techniques. Our results also demonstrate that the AC impedance method is a sensitive technique for detection of the degree of membrane hydration. Among the six cells of the stack, the center cells have lower Ohmic resistances due to high temperatures at the center. Variation of the Ohmic resistances among the individual cells is high at low currents and low at high currents. However, variation of the voltage loss due to the Ohmic resistance is higher at high currents. This is the reason that there are more “low cells” at high current operation.

Acknowledgement

The authors gratefully acknowledge the National Fuel Cell program of National Research Council Canada for financially supporting this project.

References

[1] A.G. Hombrados, L. Gonzalez, M.A. Rubio, W. Agila, E. Villanueva, D. Guinea, E. Chinarro, B. Moreno, J.R. Jurando, J. Power Sources 151 (2005) 25–31.
[2] C. Brunetto, G. Tina, G. Squadrito, A. Moschetto, in: M. Matijasevic, B. Pejcinovic, Z. Tomsic, Z. Butkovic (Eds.), Proceedings of the 12th IEEE Mediterranean Electrochemical conference, IEEE, Piscataway, NJ, 12–15 May, 2004, pp. 1045–1050.
[3] N. Wagner, J. Appl. Electrochem. 32 (2002) 859–863.
[4] T. Romero-Castanon, L.G. Arriaga, U. Cano-Castillo, J. Power Sources 118 (2003) 179–182.
[5] K. Jae-Dong, I.P. Yong, K. Kobayashi, M. Nagai, M. Kunimatsu, Solid State Ionics, Diffus. React. 140 (2001) 313–325.
[6] N. Wagner, E. Gulzow, J. Power Sources 127 (2004) 341–347.
[7] F. Lufrano, P. Staiti, M. Minuroli, J. Power Sources 124 (2003) 314–320.
[8] M. Eikerling, A.A. Kornyshev, J. Electroanal. Chem. 475 (1999) 107–123.
[9] J.M. Song, S.Y. Cha, W.M. Lee, J. Power Sources 94 (2001) 78–84.
[10] Q. Guo, M. Cayetano, Y. Tsou, E.S. De-Castro, R.E. White, J. Electrochem. Soc. 150 (2003) A1440–A1449.
[11] T.E. Springer, T.A. Zawodzinski, M.S. Wilson, S. Gottesfeld, J. Electrochem. Soc. 143 (1996) 587–599.
[12] G. Li, P.G. Pickup, J. Electrochem. Soc. 150 (2003) C745–C752.
[13] B. Andreaus, A.J. McEvoy, G.G. Scherer, Electrochim. Acta 47 (2002) 2223–2229.
[14] T.J.P. Freire, E.R. Gonzalez, J. Electroanal. Chem. 503 (2001) 57–68.
[15] T. Abe, H. Shima, K. Watanabe, Y. Ito, J. Electrochem. Soc. 151 (2004) A101–A105.
[16] T.E. Springer, T.A. Zawodzinski, M.S. Wilson, S. Gottesfeld, in: S. Gottesfeld, G. Halpert, A. Landgrebe (Eds.), Proceedings of the First International Symposium on Proton Conducting Membrane Fuel Cells, Electrochem. Soc., Pennington, NJ, 1–8 October, 1995, pp. 137–151.
[17] J.D. Halla, M. Mamak, D.E. Williams, G.A. Ozin, Adv. Funct. Mater. 13 (2003) 133–138.
[18] M. Ciureanu, M. Badita, J. New Mater. Electrochem. Syst. 6 (2003) 163–168.
[19] H.C. Young, G.S. Yong, C.C. Won, I.W. Seong, S.H. Hak, J. Power Sources 118 (2003) 334–341.
[20] R. Halseid, P.J.S. Vie, R. Tunold, J. Electrochem. Soc. 151 (2004) A381–A388.
[21] S. Slade, S.A. Campbell, T.R. Ralph, F.C. Walsh, J. Electrochem. Soc. 149 (2002) A1556–A1564.
[22] F. Damay, L.C. Klein, Solid State Ionics, Diffus. React. 162–163 (2003) 261–267.
[23] A. Sen, K.E. Leach, R.D. Varjian, in: D.H. Doughty, B. Vyas, T. Takamura, J.R. Huff (Eds.), Symposium of Materials for Electrochemical Energy Storage and Conversion—Batteries, Capacitors and Fuel Cells, Mater. Res. Soc., Philadelphia, PA, 17–20 April, 1995, pp. 157–162.
[24] R.F. Suva, M. De-Francesco, A. Pozio, J. Power Sources 134 (2004) 18–26.
[25] B. Andreaus, G.G. Scherer, Solid State Ionics, Diffus. React. 168 (2004) 311–320.
[26] J.D. Kim, Y. Park, K. Kobayashi, M. Nagai, J. Power Sources 103 (2001) 127–133.
[27] M. Ciureanu, H. Wang, J. Electrochem. Soc. 146 (1999) 4031–4040.
[28] M. Ciureanu, J. Appl. Electrochem. 34 (2004) 705–714.
[29] J.P. Diard, N. Glandut, B. Le-Gorrec, C. Montella, J. Electrochem. Soc. 151 (2004) A2193–A2197.
[30] G. Bender, M.S. Wilson, T.A. Zawodzinski, J. Power Sources 123 (2003) 163–171.
[31] D.J.L. Brett, S. Atkins, N.P. Brandon, V. Vesovic, N. Vasileiadis, A. Kucernak, Electrochem. Solid-State Lett. 6 (2003) A63–A66.
[32] X. Yuan, J.C. Sun, M. Blanco, H. Wang, J. Zhang, D.P. Wilkinson, J. Power Sources 161 (2006) 920–928.
[33] D. Webb, S. Mϕller-Holst, J. Power Sources 103 (2001) 54–60.
[34] T. Mennola, M. Mikkola, M. Noponen, T. Hottinen, P. Lund, J. Power Sources 112 (2002) 261–272.
[35] T.E. Springer, T.A. Zawodzinski, M.S. Wilson, S. Gottesfeld, J. Electrochem. Soc. 143 (1996) 587–599.
[36] T. Romero-Castanon, L.G. Arriaga, U. Cano-Castillo, J. Power Sources 118 (2003) 179–182.
[37] A. Fischer, J. Jindra, H. Wendt, J. Appl. Electrochem. 28 (1998) 277–282.
[38] N. Wagner, E. Gulzow, J. Power Sources 127 (2004) 341–347.

[39] P. Godea, F. Jaouen, G. Lindbergh, A. Lundblad, G. Sundholm, Electrochim. Acta 48 (2003) 4175–4187.
[40] F. Jaouen, G. Lindbergh, K. Wiezell, J. Electrochem. Soc. 150 (2003) A1711–A1717.
[41] F. Lu, B. Yi, D. Xing, J. Yu, Z. Hou, Y. Fu, J. Power Sources 124 (2003) 81–89.
[42] T.J.P. Freire, E.R. Gonzalez, J. Electroanal. Chem. 503 (2001) 57–68.
[43] F.N. Büchi, G.G. Scherer, J. Electroanal. Chem. 404 (1996) 37–43.
[44] M. Eikerling, Yu.I. Kharkats, A.A. Kornyshevf, Yu.M. Volfkovich, J. Electrochem. Soc. 145 (1998) 2684–2699.
[45] R.F. Mann, J.C. Amphlett, M.A.I. Hooper, H.M. Jensen, B.A. Peppley, P.R. Roberge, J. Power Sources 86 (2000) 173–180.
[46] F.N. Büchi, G.G. Scherer, J. Electrochem. Soc. 148 (2001) A183–A188.